

# Quadriwave lateral shearing interferometer based on a randomly encoded hybrid grating

Tong Ling, Dong Liu, Xiumei Yue, Yongying Yang,\* Yibing Shen, and Jian Bai

State Key Laboratory of Modern Optical Instrumentation, Department of Optical Engineering, Zhejiang University, 38 Zheda Road, Hangzhou 310027, China

\*Corresponding author: chuyyy@zju.edu.cn

Received March 16, 2015; revised April 5, 2015; accepted April 17, 2015;  
posted April 20, 2015 (Doc. ID 236118); published May 6, 2015

A compact quadriwave lateral shearing interferometer (QWLSI) with strong adaptability and high precision is proposed based on a novel randomly encoded hybrid grating (REHG). By performing the inverse Fourier transform of the desired  $\pm 1$  Fraunhofer diffraction orders, the amplitude and phase distributions of the ideally calculated quadriwave grating can be obtained. Then a phase chessboard is introduced to generate the same phase distribution, while the amplitude distribution can be achieved using the randomly encoding method by quantizing the radiant flux on the ideal quadriwave grating. As the Fraunhofer diffraction of the REHG only contains the  $\pm 1$  orders, no order selection mask is ever needed for the REHG-LSI. The simulations and the experiments show that the REHG-LSI exhibits strong adaptability, nice repeatability, and high precision. © 2015 Optical Society of America

OCIS codes: (120.0120) Instrumentation, measurement, and metrology; (120.3180) Interferometry; (050.1950) Diffraction gratings; (120.5050) Phase measurement.

<http://dx.doi.org/10.1364/OL.40.002245>

Compared to conventional interferometers like Fizeau and Twyman-Green interferometers, multilateral shearing interferometers (multi-LSIs) are compact and stable. Moreover, thanks to the common-path configuration, multi-LSIs can be applied to the transient wavefront testing or the aberration measurement of highly precise projection optics for very large scale integration (VLSI) [1,2]. Commonly used multi-LSIs include the cross-grating lateral shearing interferometer (CGLSI) [3], the three-wave lateral shearing interferometer (TWLSI) [4], and the quadriwave lateral shearing interferometer (QWLSI) based on the modified Hartmann mask (MHM) [5]. The CGLSI consists of a cross-grating and an order selection mask to select the  $\pm 1$  orders for lateral shearing interference, and their fabrication is relatively simple. It can be employed to test the wavefront of convergent beams directly and the wavefront of collimated beams with an aplanatic lens [6]. However, in order to reduce the system error, the cross-grating needs to be as close as possible to the order selection mask, which makes it difficult to adjust the position of each component. Besides, as the distance between order selection windows precisely corresponds to the focal length of the wavefront under test, the order selection mask actually limits the testing range of the CGLSI. The MHM introduces a phase chessboard on the basis of a cross-grating, and the even orders and the multiples of 3 orders are then eliminated. The diffraction efficiency of the  $\pm 1$  orders is better, but the  $\pm 5$  and  $\pm 7$  orders also remain in the diffractions. If there is no order selection mask employed to help selecting the  $\pm 1$  orders, the wavefront will be measured in the approach regarding the MHM as a Hartmann sensor only at the Talbot distance [7]. And the resolution is also limited compared to the derivation by Chanteloup and Cohen [8], the ideal QWLSI, which contains only 4 beams in two orthogonal directions, can be realized by combining a phase chessboard with an amplitude grating whose transmittance distribution is the absolute value of cosine function. However, this grating is difficult to be made, as the same

variation of intensity cannot be easily obtained by general grating fabrication methods.

In this Letter, a QWLSI with strong adaptability and high precision based on a randomly encoded hybrid grating (REHG) is proposed, which makes it possible to achieve quadriwave lateral shearing interference among only four diffraction beams without the introduction of an order selection mask. The REHG-LSI is very compact. It only consists of a REHG and a CCD. Figure 1 shows the optical layout of our REHG-LSI for collimated beam wavefront testing, where the REHG is a grating with both amplitude and phase modulation approximate to the ideally calculated quadriwave grating. Once the beam under test hits the REHG, it will be diffracted into only four beams on the angle bisectors between the  $x$  axis and the  $y$  axis. Finally, these beams will reach the imaging plane and form a quadriwave lateral shearing interferogram in their overlapped region on the CCD. The spacing from the grating to the CCD is determined to make sure that the interferogram completely fills the field of view.

In detail, the REHG consists of a phase chessboard and a randomly encoded binary amplitude grating, as is shown in Fig. 2. The phase chessboard is a transparent substrate on which the phase modulation of 0 and  $\pi$  arrange alternatively, and the binary amplitude grating simulates the transmittance of the ideal quadriwave grating with tiny encoded pixels of mask. The grating pitch of the binary amplitude grating is a half of the pitch of the phase

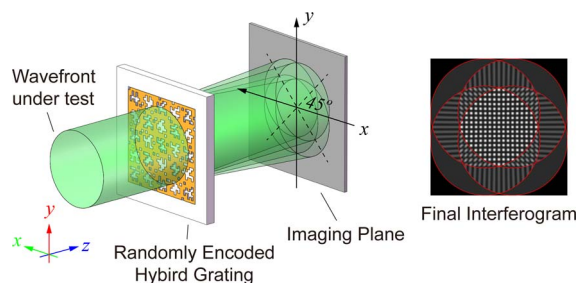


Fig. 1. Optical layout of the REHG-LSI for wavefront testing.

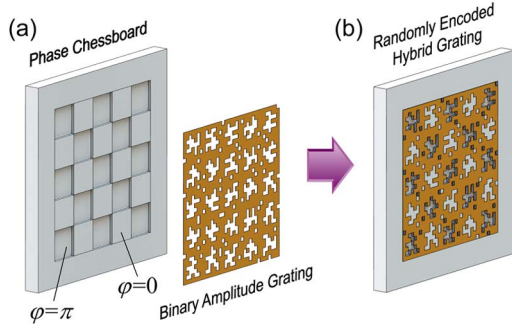


Fig. 2. Schematic diagram of the REHG structure.

chessboard. Due to the combined effect of the phase chessboard and the binary amplitude grating, the beam passing through the REHG will only be diffracted into the  $\pm 1$  orders in two orthogonal directions. And there is no need to employ an order selection mask, which, as a result, not only makes the system more compact and portable, but also enlarges the testing range of wavefront distortion compared to the CGLSI.

The REHG is based on the ideally calculated quadriwave grating that only has the  $\pm 1$  diffraction orders in two orthogonal directions. Assume that the transmittance of this ideal grating is  $t_{id}(x, y)$ , its Fourier transform  $T_{id}(u, v)$ , which also represents the Fraunhofer diffraction when a collimated beam is incident on this grating, should contain the following orders [8]:

$$T_{id}(u, v) = \delta(u - u_0, v - v_0) + \delta(u - u_0, v + v_0) + \delta(u + u_0, v - v_0) + \delta(u + u_0, v + v_0), \quad (1)$$

where  $u, v$  are, respectively, the spatial frequencies in the  $x$  and  $y$  directions, and  $u_0, v_0$  represent the peaks of the  $\pm 1$  orders. The transmittance  $t_{id}(x, y)$  can be obtained by performing inverse Fourier transform of Eq. (1),

$$t_{id}(x, y) = \cos(2\pi u_0 x) \cos(2\pi v_0 y). \quad (2)$$

In general, the peak frequencies  $u_0$  and  $v_0$  in the  $x$  and  $y$  directions are the same. And according to the definition of the period or pitch of grating, the pitch  $d$  of the ideal quadriwave grating is

$$d = \frac{1}{u_0} = \frac{1}{v_0}. \quad (3)$$

Substituting Eq. (3) into Eq. (2), the transmittance of the ideal grating can be expressed as

$$t_{id}(x, y) = \cos\left(\frac{2\pi x}{d}\right) \cos\left(\frac{2\pi y}{d}\right). \quad (4)$$

The cosine function here ranges from  $-1$  to  $1$ , so does the transmittance. As the negative transmittance cannot be obtained from a simple amplitude grating, Eq. (4) is decomposed into its signal multiplied by its absolute value:

$$t_{id}(x, y) = \text{sgn}(t_{id}(x, y)) \cdot |t_{id}(x, y)|. \quad (5)$$

From this derivation, the signal distribution  $\text{sgn}(t_{id}(x, y))$  can be obtained from a phase chessboard with  $0$  and  $\pi$  phase modulation. Therefore, the phase distribution can be described as

$$\varphi_{\text{phase}}(x, y) = \pi \cdot \left[ \text{rect}\left(\frac{2x}{d}\right) * \text{comb}\left(\frac{x}{d}\right) \right] \times \left[ \text{rect}\left(\frac{2y}{d}\right) * \text{comb}\left(\frac{y}{d}\right) \right]. \quad (6)$$

For the amplitude distribution, conventional methods of making cosine amplitude grating would employ holography or interferometry to obtain cosine intensity distribution. However, the ideally calculated amplitude transmittance here does not fully fit the cosine distribution, but complies with the absolute value of the cosine distribution, that is,

$$t_{\text{amp}}(x, y) = \left| \cos\left(\frac{2\pi x}{d}\right) \cos\left(\frac{2\pi y}{d}\right) \right|. \quad (7)$$

To obtain such intensity distribution is difficult for conventional approaches. Therefore, a randomly encoded binary amplitude grating is proposed based on the quantization of the radiant flux on the ideal quadriwave grating. The designing process of this binary amplitude grating is made up of three steps, which are grid division, quantization, and randomly encoding.

In the beginning, the amplitude transmittance of the ideally calculated quadriwave grating is divided equally into  $N \times N$  grids, and each grid will be further subdivided into  $M \times M$  square pixels. As is shown in Fig. 3(a), the transmittance of the pixel  $(i, j)$  can be expressed as

$$t_{\text{amp}}(x_i, y_j) = \left| \cos\left(\frac{2\pi x_i}{d}\right) \cos\left(\frac{2\pi y_j}{d}\right) \right|, \quad i, j \in [1, N \times M] \cap \mathbb{Z}. \quad (8)$$

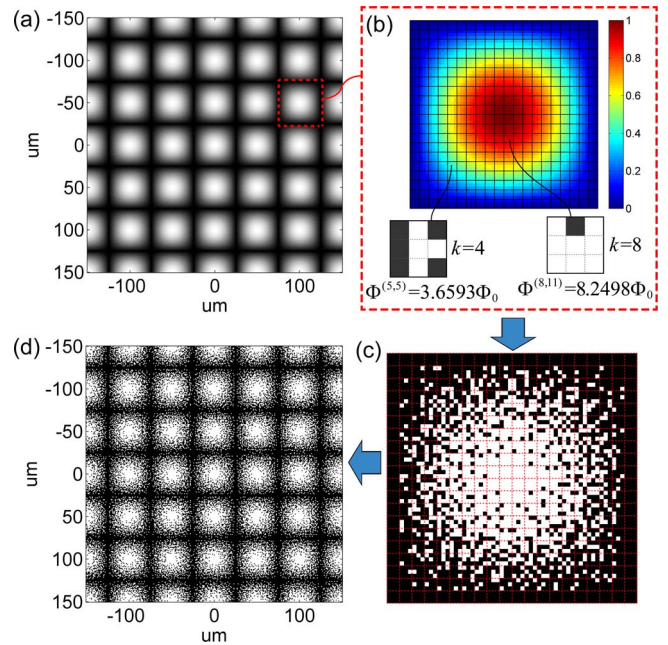


Fig. 3. Flowchart of the randomly encoding method based on the quantization of radiant flux for REHG designing, (a) the amplitude transmittance of the ideal quadriwave grating, (b) quantizing the radiant flux in each grid and randomly encoding the value of the pixels by the corresponding quantization level of the grid when  $M = 3$ , (c) the binary transmittance distribution in one period, (d) the binary transmittance distribution in the area from  $-150$  to  $150 \mu\text{m}$  on the REHG whose pitch is  $100 \mu\text{m}$ .

Next, the step of quantization is to convert the total radiant flux in each grid into different quantization levels. Assume that the radiant flux fully crossing a single pixel is  $\Phi_0$ , then the total radiant flux in an arbitrary grid can be obtained as

$$\Phi^{(\xi,\eta)} = \Phi_0 \sum_{p=1}^M \sum_{q=1}^M t_{\text{amp}}(x_{M\xi-M+p}, y_{M\eta-M+q}), \quad (9)$$

where  $(\xi, \eta)$  is the grid coordinate. Once the radiant flux in each grid on the ideal grating is obtained, the total number of the quantization levels should be determined afterward. As the pixel on the binary amplitude grating we are designing can only have two values, 1 and 0, which imply the transmittance of the current pixel, 1 means the pixel is transparent, while 0 means the light cannot pass through. Then all the possibilities of the total radiant flux in one grid will have  $M^2 + 1$  different cases from 0 to  $M^2$ . As a result, the radiant flux in Eq. (9) should also be uniformly quantized at  $M^2 + 1$  quantization levels, that is,

$$\hat{\Phi}^{(\xi,\eta)} = k\Phi_0, \quad (k - 1/2)\Delta \leq \Phi^{(\xi,\eta)} < (k + 1/2)\Delta, \quad (10)$$

where  $k = 0, 1, \dots, M^2$ , and  $\Delta$  is the quantization step between two adjacent levels, which is exactly  $\Phi_0$ . As the radiant flux of the pixel valued 1 is also  $\Phi_0$ , the quantization level  $k$  actually stands for the number of the pixels whose value is 1 in one grid. Figure 3(b) shows that in Grid (5,5) and Grid (8,11), there should be, respectively, 4 pixels and 8 pixels assigned 1 when  $M = 3$ , where the pixels assigned 1 are white, while the pixels assigned 0 are black.

Every pixel on the binary amplitude grating will then be encoded with 1 and 0 in Fig. 3(c). It should be noted that the number of the pixels assigned 1 in each grid should be fixed to the quantization level  $k$ , but the pattern of these pixels should be random, and the purpose of employing random pattern is to avoid introducing extra diffraction orders due to the periodicity of local structure. Utilizing this randomly encoding process to all the pixels in each grid, the final transmittance distribution of the binary amplitude grating can be obtained in Fig. 3(d), where  $N = 100$  and  $M = 3$ .

Combining this amplitude grating with a phase chessboard, a mathematic model of the amplitude and phase modulation of a REHG is built. Then the normalized intensity of the Fraunhofer diffraction orders can be calculated out by fast Fourier transform (FFT). The comparison of the normalized intensity of Fraunhofer diffraction orders between different gratings, which are, respectively, the ideally calculated quadriwave grating, the phase chessboard, the MHM, and the REHG, is shown in Fig. 4. It is obvious that the MHM suppresses several orders like  $\pm 3$  and  $\pm 9$  on the basis of a phase chessboard, but the REHG successfully eliminates all the other orders except the only  $\pm 1$  orders, which is very similar to the ideal quadriwave grating. One of the few differences of their diffractions in Fig. 4 is that the Fraunhofer diffraction of the REHG contains a base intensity everywhere like the white noise, owing to the randomly encoding process. But this base intensity, which is only 0.015

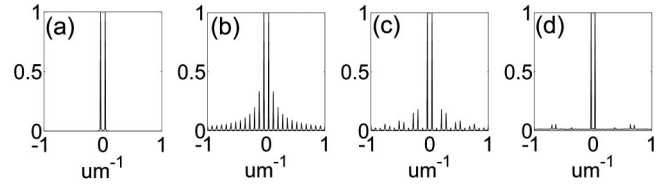


Fig. 4. Normalized intensity of Fraunhofer diffraction orders with different gratings, (a) the ideally calculated quadriwave grating, (b) the phase chessboard, (c) the MHM, (d) the REHG.

compared to the  $\pm 1$  orders, is so weak that it can be neglected.

In our simulation, the theory of Fresnel diffraction is introduced [6] and an Nvidia GTX780 graphics card with the technology of CUDA, which can reduce our computing time from one day to nearly 10 seconds and enlarge the simulation scale to a practical size of millimeters, is employed. Thus it is possible for us to simulate the interference patterns of arbitrary wavefronts passing through different gratings. Figure 5 shows the change of interferogram when the image plane is set at 13.5, 17, 20.5, 24, and 27.5 mm away from the phase chessboard, the MHM, and the REHG. Due to the interaction between different diffraction orders, the interference patterns obtained by the phase chessboard and the MHM both vary with the distance change periodically. However, the interferogram obtained by the REHG is more stable as the imaging distance changes, and all the distance is suitable for quadriwave lateral shearing interference. As the imaging distance monotonously changes with the shear ratio, the selection of the shear ratio with REHG is also more flexible. In fact, these features imply the strong adaptability of the REHG-LSI. Users just need to set a REHG and a CCD anywhere convenient in the optical path, and the quadriwave interferogram will be easily obtained.

To validate the precision of our REHG-LSI, a REHG whose pitch is 240  $\mu\text{m}$  is employed to test the wavefront distortion of an  $\phi 5$  mm optical flat in comparison with a ZYGO GPI interferometer. The REHG is 6.6 mm  $\times$  6.6 mm in size, the grid number  $N = 1100$ , and the subdivision number  $M = 3$ , which means that the pixel size on the grating is set to 2  $\mu\text{m}$ . The picture of the actual REHG is shown in Fig. 6. The phase chessboard of the

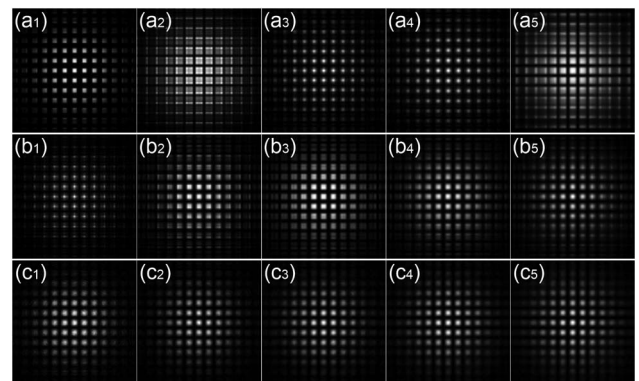


Fig. 5. Change of interferograms when observed at 13.5, 17, 20.5, 24, and 27.5 mm with the grating of (a<sub>1</sub>)–(a<sub>5</sub>) the phase chessboard, (b<sub>1</sub>)–(b<sub>5</sub>) the MHM, and (c<sub>1</sub>)–(c<sub>5</sub>) the REHG. Media 1, 2, and 3 show the detailed variation with these three gratings, respectively.

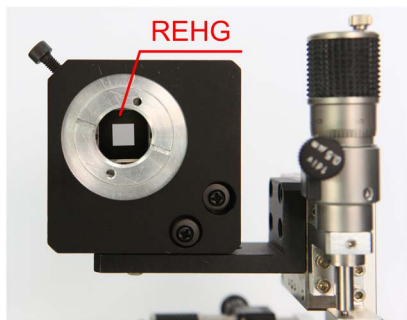


Fig. 6. Actual REHG mounted on the precision linear stages.

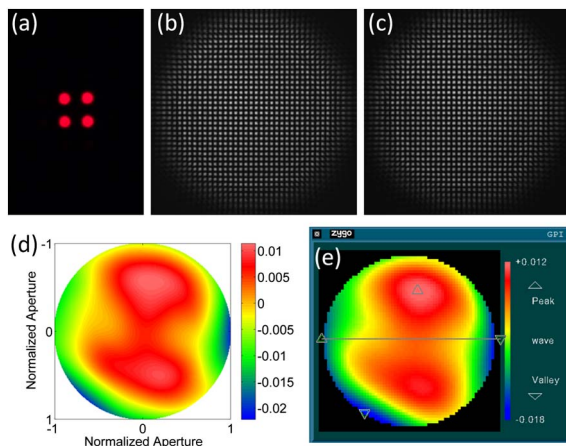


Fig. 7. Comparative experiment results with a ZYGO GPI, (a) the only four diffractions observed in the far field, (b) the interferogram of the collimated beam, (c) the interferogram of the collimated beam passing through the optical flat, (d) the wavefront distortion of the optical flat retrieved by the REHG-LSI, (e) the testing result of the same optical flat with a ZYGO GPI.

REHG is made by reactive ion etching (RIE) on the fused silica substrate, while the randomly encoded binary amplitude grating is fabricated by electron beam lithography (EBL) on the chrome mask.

At the beginning of the experiment, we let the beam from a collimator directly pass through the REHG, and only four diffraction beam spots are observed in the far field as in Fig. 7(a). The interferogram of the collimator is obtained for system error calibration in Fig. 7(b), and the coating wavelength of this collimator is 632.8 nm. Then the interferogram of the collimated beam going through the optical flat is obtained in Fig. 7(c). As the simulation above also suggests, these interferograms keep very stable with nice repeatability during the whole experiment and are flexible of selecting different shear ratios at different imaging distances. In the data processing procedure, the FFT method [9] is employed at first to extract the shearing wavefronts in two orthogonal directions from the interferogram obtained by the REHG. And with the help of differential Zernike polynomial fitting method [10,11], the wavefront under test can be further retrieved, as is shown in Fig. 7(d), whose peak-to-valley (PTV) is  $0.034\lambda$  and root-mean-square (RMS) is  $0.007\lambda$ . Figure 7(e) shows the result of the same optical flat with a ZYGO GPI interferometer. The PTV is  $0.030\lambda$ , and the RMS is  $0.006\lambda$ . In this comparison with the ZYGO GPI,

the REHG-LSI achieves the PTV error of  $0.004\lambda$  and the RMS error of  $0.001\lambda$ , which is highly precise.

In conclusion, a compact QWLSI with both strong adaptability and high precision based on an REHG is proposed. By performing the inverse Fourier transform of the desired  $\pm 1$  Fraunhofer diffraction orders, the amplitude and phase distributions of the ideally calculated quadriwave grating can be obtained. Then a phase chessboard is introduced to generate the same phase distribution, while the amplitude distribution can be achieved using randomly encoding method. In this method, the ideally calculated amplitude distribution is first divided into discrete grids. And the total radiant flux in each grid needs to be quantized in several quantization levels. A binary amplitude grating is then generated by encoding the pixels in the grids with 0 and 1 so that the total radiant flux in each grid on this binary amplitude grating approximate to the flux in the corresponding grid on the ideal quadriwave grating. In addition, random pattern is employed in the encoding process to avoid introducing extra diffraction orders. The Fraunhofer diffraction orders of the REHG are very similar to the diffractions of the ideal quadriwave grating, which only contain the  $\pm 1$  orders, thus no order selection mask is ever needed. The simulations and the experiments show that the REHG-LSI exhibits strong adaptability, nice repeatability, and high precision. As the REHG-LSI is also very compact and portable, it can be employed in many fields like optics fabrication and high precision wavefront diagnosis *in situ*.

This work was partially supported by the National Natural Science Foundation of China (11275172, 61475141, 41305014), Zhejiang Province Education Department Scientific Research Program (Y201329660), the Specialized Research Fund for the Doctoral Program of Higher Education of China (20130101120133), Zhejiang Key Discipline of Instrument Science and Technology (JL130113), the State Key Lab. of MOI Innovation Program (MOI2015QN01), and the Aviation Science Funds (20140376001).

## References

1. S. Kato, C. Ouchi, M. Hasegawa, A. Suzuki, T. Hasegawa, K. Sugisaki, M. Okada, Z. Yucong, K. Murakami, J. Saito, M. Niibe, and M. Takeda, Proc. SPIE **5751**, 110 (2005).
2. S. Velghe, J. Primot, N. Guérineau, M. Cohen, and B. Wattellier, Opt. Lett. **30**, 245 (2005).
3. C. Ouchi, S. Kato, M. Hasegawa, T. Hasegawa, H. Yokota, K. Sugisaki, M. Okada, K. Murakami, J. Saito, M. Niibe, and M. Takeda, Proc. SPIE **6152**, O1522 (2006).
4. J. Primot, Appl. Opt. **32**, 6242 (1993).
5. J. Primot and N. Guérineau, Appl. Opt. **39**, 5715 (2000).
6. T. Ling, Y. Yang, X. Yue, D. Liu, Y. Ma, J. Bai, and K. Wang, Appl. Opt. **53**, 7144 (2014).
7. W. Boucher, P. Delage, and B. Wattellier, Proc. SPIE **8082**, 80821E (2011).
8. J.-C. F. Chanteloup and M. Cohen, Proc. SPIE **5252**, 282 (2004).
9. M. Takeda, H. Ina, and S. Kobayashi, J. Opt. Soc. Am. **72**, 156 (1982).
10. F. Dai, F. Tang, X. Wang, O. Sasaki, and P. Feng, Appl. Opt. **51**, 5028 (2012).
11. T. Ling, D. Liu, L. Sun, Y. Yang, and Z. Cheng, Proc. SPIE **8838**, 88380J (2013).